Catalysis Science & Technology

PAPER

View Article Online
View Journal | View Issue

Cite this: *Catal. Sci. Technol.*, 2014, **4**, 3524

Mechanistic examination of Au^{III}-mediated 1,5-enyne cycloisomerization by $AuBr_2$(*N*-imidate)(NHC)/AgX precatalysts – is the active catalyst Au^{III} or Au^{I}?†

Jonathan P. Reeds,[a] Mark P. Healy‡[b] and Ian J. S. Fairlamb*[a]

Received 12th May 2014,
Accepted 3rd July 2014

DOI: 10.1039/c4cy00617h

www.rsc.org/catalysis

Gold(III) catalysts mediate 1,5-enyne cycloisomerization or tandem nucleophilic substitution-1,5-enyne cycloisomerization processes in an efficient manner. This study examines the reaction kinetics of 1,5-enyne cycloisomerization, mediated by $AuBr_2$(*N*-imidate)(NHC) catalysts {where *N*-imidate = *N*-tetrafluorosuccinimide (*N*-TFS) or *N*-phthalimide (*N*-phthal) and NHC = *N*,*N*′-di-*tert*-pentylimidazol-2-ylidene (I^tPe)}, in the presence of AgOTf, in comparison with $Au^{III}Br_3$(NHC) and $Au^{I}Br$(NHC). The nature of *N*-imidate anion influences catalyst efficacy. NMR spectroscopic investigations have allowed the ease of reduction of $AuBr_2$(*N*-TFS)(NHC) to $Au^{I}X$(NHC) (where X = *N*-TFS or Br) to be examined. Br_2 is liberated from Au^{III}, which has been trapped by a sacrificial alkene. Under working catalyst conditions cationic Au^{III} is reduced to Au^{I}.

Introduction

Organic transformations catalysed by Au species are of current interest within both the synthetic chemistry and catalysis communities.[1] Of the reaction classes, 1,*n*-enyne cycloisomerization processes (*n* = 5 and 6) have attracted notable attention.[2] While several transition metals are able to affect 1,*n*-enyne substrates, Au occupies a special position in this arena,[2,3] as an eclectic array of structurally diverse organic products can be formed, depending on the catalyst and substrate identities, in addition to the reaction conditions used.

1,6-Enyne cycloisomerization processes generally involve 6-*exo*-dig cyclization and are mechanistically well understood.[4] 1,5-Enyne cycloisomerization processes, involving 5-*endo*-dig cyclization, have not been examined to the same extent, despite the numerous synthetic possibilities. Nevertheless, several catalyst manifolds are known to deliver different products depending on the electronic character of the Au centre (see Scheme 1 for selected examples). This prompted Sun and Lin to explore the mechanisms of 1,5-enyne cycloisomerization, mediated by Au^{I}, by DFT calculations (B3LYP).[5]

In an earlier study we developed a tandem nucleophilic substitution-1,5-enyne cycloisomerization process (**5** → **8**),[6] starting from propargyl alcohol (**5**) and allyl silane (**6**), to deliver bicyclo[3.1.0]hexene products (**8**). For this process, $Au^{III}Br_2$(*N*-TFS)(I^tPe) in combination with the non-coordinating anion, Ag[Al(OC(CF_3)$_3$)$_4$], proved an active and selective catalyst for the tandem process. By comparison with $Au^{I}Br$(I^tPe) (note: near-inactive for the tandem process), it was shown that a Au^{III} species was required for the initial nucleophilic substitution reaction. However, a question that arose from the study was the nature of the active catalyst species in the cycloisomerization step, *i.e.* is Au^{III} or Au^{I} responsible for cycloisomerization?

In this paper we examine the reaction kinetics of 1,5-enyne cycloisomerization, mediated by $AuBr_2$(*N*-imidate)

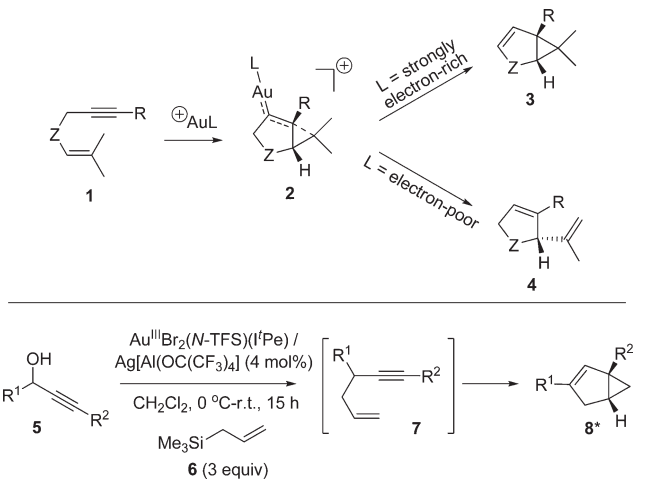

Scheme 1 Top: 1,5-enyne cycloisomerization showing how L can direct selectivity (**3** & **4** representative products; others possible). Bottom: a tandem nucleophilic substitution-1,5-enyne cycloisomerization – thermal 1,3-rearrangements are possible for **8** (R^1/R^2 = aryl groups).

[a] *Department of Chemistry, University of York, Heslington, York YO10 5DD, UK. E-mail: ian.fairlamb@york.ac.uk*
[b] *GlaxoSmithKline, New Frontiers Science Park, Third Avenue, Harlow, Essex CM19 5AW, UK*

† Electronic supplementary information (ESI) available: Representative NMR spectra and other characterization data. See DOI: 10.1039/c4cy00617h

‡ Novartis Pharmaceuticals UK Limited, Horsham Research Centre, Wimblehurst Road, GB-Horsham, West Sussex RH12 5AB, U.K.

(NHC) catalysts {where *N*-imidate = *N*-tetrafluorosuccinimide (*N*-TFS) or *N*-phthalimide (*N*-phthal) and NHC = *N*,*N*′-di-*tert*-pentylimidazol-2-ylidene (I^{t}Pe)} in the presence of AgOTf. The findings allow an understanding of 1,5-enyne substrate turnover, indicating that catalyst decomposition is an issue for certain catalysts. It has been found that the *N*-imidate anion plays a stabilizing role for effective catalysis. NMR spectroscopic investigations have been used to examine the degradation of Au^{III} to Au^{I}, which support the kinetic studies.

Results and discussion

The study is divided into two parts: (a) kinetic investigations; (b) NMR spectroscopic investigations.

(a) Kinetic investigations

The 1,5-enyne cycloisomerization reaction (**9** → **10**) examined in these kinetic investigations is shown in Scheme 2, which has previously been validated as a useful benchmark reaction[6b] for testing Au catalyst efficacy (the reaction is selective for **10** and negligible side-reactions are seen).

The catalysts used in this study are collated in Fig. 1, which were selected from a wider library of catalysts previously reported by our group.[6a,b]

The reaction of **9** → **10** was monitored by HRGC analysis. The response factors are near identical for **9** and **10** (authenticated by ^{1}H NMR spectroscopic analysis), which is expected as they are isomers. The conversion of pure **9** (ascertained by ^{1}H NMR spectroscopy) and associated kinetic profile is shown in Fig. 2 for the reaction mediated by 1 mol% $AuBr_2$(*N*-TFS)(I^{t}Pe), in the presence of either 1 or 2 mol% AgOTf in DCE at 25 °C. The first equivalent (relative to Au cat.) serves to abstract bromide from $AuBr_2$(*N*-TFS)(I^{t}Pe) forming [AuBr(*N*-TFS)(I^{t}Pe)]OTf and AgBr *in situ*. The second equivalent of AgOTf could in principle abstract another bromide.

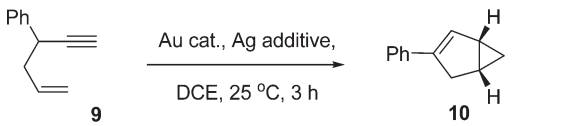

Scheme 2 1,5-Enyne cycloisomerization reaction for the kinetic investigations.

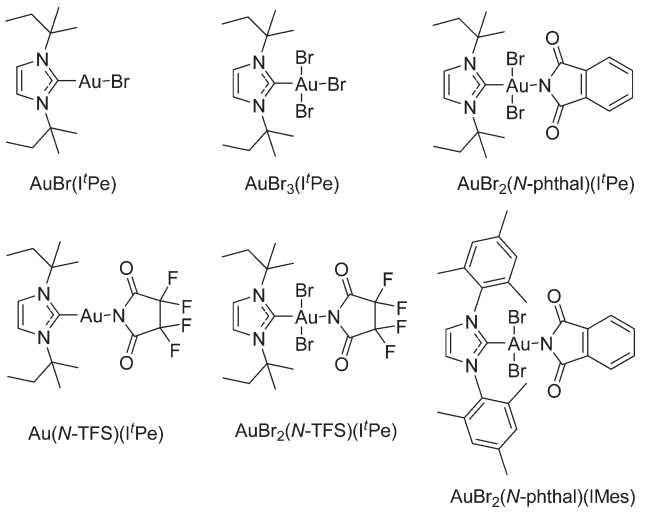

Fig. 1 The structures of the catalysts used in this mechanistic study.

Examination of the kinetic profiles in Fig. 2 indicate that there is no benefit in an additional equivalent of AgOTf. Both AgOTf and $AuBr_2$(*N*-TFS)(I^{t}Pe) are necessary for active catalysis (confirmed by control experiments). The data generated by HRGC could be fitted to a pseudo-first order rate equation using Dynafit™ (by curve fitting; regression analysis of ln[enyne] *vs.* time afforded similar data), which allowed the observed rate (k_{obs}) and initial rate to be determined.[7] For the reaction where the $AuBr_2$(*N*-TFS)(I^{t}Pe) : AgOTf was 1 : 1, it was determined that $k_{obs} = 3.14 \times 10^{-4}$ s^{-1} and the initial rate (T_0) = 6.28×10^{-5} moldm^{-3} s^{-1} (standard error = 2.5%). A marginally faster reaction was recorded when the ratio was 1 : 2 ($k_{obs} = 4.16 \times 10^{-4}$ s^{-1}; $T_0 = 8.32 \times 10^{-5}$ moldm^{-3} s^{-1}; standard error = 3.3%).

Based on these data the ratio of the Au catalyst to Ag additive was maintained at 1 : 1 for all subsequent reactions, which is in-keeping with the ratio commonly used for many related cycloisomerization processes.

The kinetic profiles for the conversion of **9** (by HRGC), catalyzed by five different Au catalysts, are shown in Fig. 3. The kinetic data is collated in Table 1. AuBr(I^{t}Pe), $AuBr_2$(*N*-TFS)(I^{t}Pe), $AuBr_2$(*N*-phthal)(I^{t}Pe) and $AuBr_2$(*N*-phthal)(IMes) show reasonable first order behaviour in **9**. The catalyst showing the highest observed rate is AuBr(I^{t}Pe) ($k_{obs} = 13.98 \times 10^{-4}$ s^{-1}), which has an initial rate commensurate with $AuBr_3$(I^{t}Pe) ($T_0 = 27.96 \times 10^{-5}$ moldm^{-3} s^{-1} and 21.87×10^{-5},

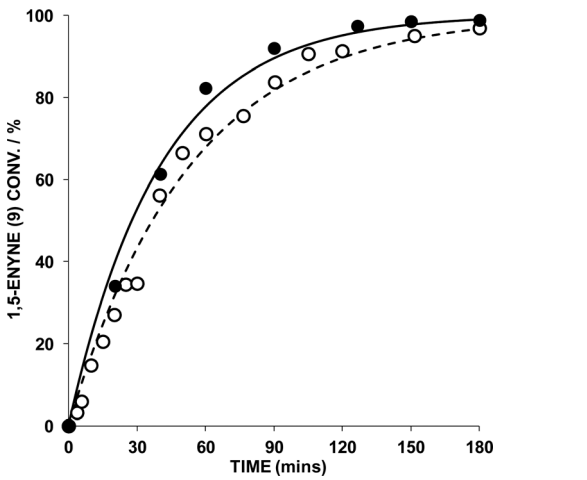

Fig. 2 Effect of AgOTf equivalents relative to $AuBr_2$(*N*-TFS)(I^{t}Pe) in 1,5-enyne cycloisomerisation of **9** (key: ● = 2 mol% AgOTf; ○ = 1 mol%. AgOTf). Other details: [**9**] = 0.2 M, DCE, 1 mol% Au cat., 25 °C; 1,5-enyne conversion was monitored by HRGC – each sample point was quenched by addition of N(*n*-Bu)$_4$Br. The kinetic curves were fitted using Dynafit™.

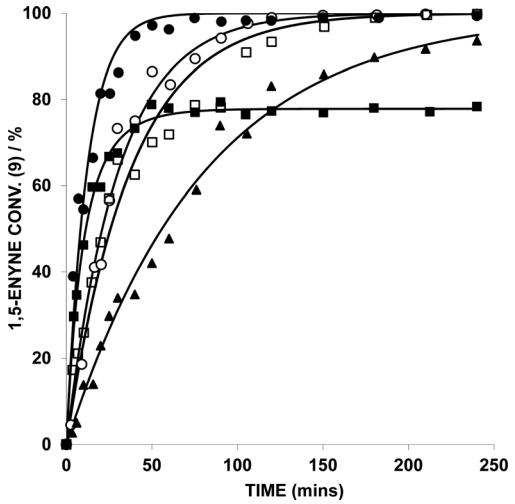

Fig. 3 Effect of 1,5-enyne concentration [**9**] on the kinetics in a reaction mediated by various Au catalysts (1 mol%), AgOTf (1 mol%), in DCE at 25 °C (key: closed circles = AuBr(I^tPe); open circles = $AuBr_2$(*N*-TFS)(I^tPe); closed squares = $AuBr_3$(I^tPe); open squares = $AuBr_2$(*N*-phthal)(I^tPe); closed triangles = $AuBr_2$(*N*-phthal)(IMes)). 1,5-Enyne conversion monitored by HRGC analysis – each sample point was quenched by addition of $(n\text{-Bu})_4$NBr. The kinetic curves were fitted using Dynafit™ with standard errors < 5%.

Table 1 Observed rate constants and initial rates for the cycloisomerization of 4-phenyl-1-hexen-5-yne (**9**) by Au^I and Au^{III} catalysts; data accompanying Fig. 3

Catalyst	$k_{obs} \times 10^{-4}$ (s^{-1})	Initial rate[a]	Error (%)
[AuBr(I^tPe)]	13.98	27.96	4.2
[$AuBr_3$(I^tPe)]	—[b]	21.87	2.3
[$AuBr_2$(*N*-TFS)(I^tPe)]	5.52	11.04	3.0
[$AuBr_2$(*N*-phthal)(I^tPe)]	4.49	8.97	4.2
[$AuBr_2$(*N*-phthal)(IMes)]	2.07	4.14	2.0

[a] Rate at $T_0 \times 10^{-5}$ ($moldm^{-3}$ s^{-1}). [b] Second order, k_{1obs} = 0.5468 mol^{-1} dm^3 s^{-1}, $k_{2obs} = 9.07 \times 10^{-4}$ s^{-1} (error 3.0%).

respectively). It is important to note that $AuBr_3$(I^tPe) did not display clean first order behaviour and catalyst deactivation is apparent after *ca.* 60 substrate turnovers. The kinetic profile could, however be fitted to a second order rate equation by curve-fitting, in which it was assumed that the Au catalyst decomposed over time and that the rate depended on both the concentration of **9** and Au catalyst.

The second order rate equation was deduced from initial rate = $k_{1obs}[enyne]_0[Au]_0 = 21.87 \times 10^{-5}$ $moldm^{-3}$ s^{-1}, where k_{1obs} (0.5468 mol^{-1} dm^3 s^{-1}) is the rate constant for the equation: **9** (1,5-enyne) + Au → Au + **10** (product). The rate of catalyst decomposition was determined by the initial rate of decomposition = $k_{2obs}[Au]_0 = 1.81 \times 10^{-6}$ s^{-1}, where k_{2obs} (9.07×10^{-4} s^{-1}) is the rate constant for the decomposition of the Au active catalyst. The inactive Au is more likely colloidal, as evidenced by the kinetic data and purple colouration of the reaction mixture.

Catalyst decomposition does not appear to hinder catalysis by the other Au^{III} complexes tested in this series. Comparison of k_{obs} for the $AuBr_2$(*N*-phthal)(I^tPe) and $AuBr_2$(*N*-phthal)(IMes) catalysts, shows that the former is twice as active as the latter (Table 1). $AuBr_2$(*N*-TFS)(I^tPe) has a marginally higher activity than $AuBr_2$(*N*-phthal)(I^tPe). It is evident that the *N*-imidate ligand could be playing a stabilizing role, when comparing *N*-imidate-containing catalysts directly with $AuBr_3$(I^tPe).

In the course of these kinetic studies it was determined that 'aged' 1,5-enyne significantly affects the kinetic profiles recorded. Aldehyde decomposition products are formed from **9** (observed by ^{1}H NMR, *ca.* 5%, after several weeks), which could interfere with the catalysis (*i.e.* slowing catalytic turnover). It was therefore found essential to employ either freshly prepared or purified **9** for the kinetic studies, which gave reproducible kinetic data.

Further examination of the catalytic behaviour of $AuBr_2$(*N*-phthal)(I^tPe) by variation of [**9**] reveals an interesting trend (Fig. 4, Table 2).

Increasing [**9**] causes a decrease in the observed rate constants, with the initial rates increasing with concentration, relating to the change in [**9**] over time. At 0.5 M [**9**] it was necessary to fit the kinetic curve to a second order rate equation, again factoring in the Au catalyst deactivation step. The observation is consistent with increasing [Au], which is concomitant with increasing [**9**]. Given these data, product inhibition and Au aggregation/decomposition are likely at higher [**9**].

A question arising from these studies is the nature of the active catalyst species. Therefore, a competition experiment was devised to discern any subtle differences in catalyst behaviour. Dimethyl allylpropargylmalonate **11** was selected as a viable 1,6-enyne benchmark substrate, which principally affords the cyclic products **12a** and **12b** (Scheme 3).

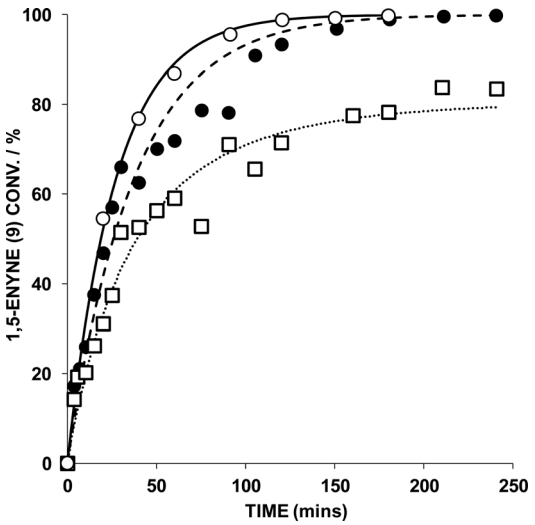

Fig. 4 Effect of 1,5-enyne concentration [**9**] in a reaction mediated by $AuBr_2$(*N*-phthal)(I^tPe) (1 mol%), AgOTf (1 mol%), in DCE at 25 °C (key: ○ = 0.1 M **9**; ● = 0.2 M **9**; □ = 0.5 M **9**). 1,5-Enyne conversion monitored by GC analysis – each sample point was quenched by addition of $(n\text{-Bu})_4$NBr. The kinetic curves were fitted using Dynafit™.

Table 2 Observed rate constants for the cycloisomerization of [9] mediated by $AuBr_2$(*N*-phthal)(I^tPe); data accompanying Fig. 4

[9] (mol dm^{-3})	$k_{obs} \times 10^{-4}$ (s^{-1})	Initial rate[a]	Error (%)
0.1	6.15	6.15	1.6
0.2	4.49	8.97	4.2
0.5	—[b]	19.20	5.7

[a] At $T_0 \times 10^{-5}$ (moldm^{-3} s^{-1}). [b] Second order $k_{1obs} = 7.68 \times 10^{-2}$ mol^{-1} dm^3 s^{-1}, $k_{2obs} = 2.36 \times 10^{-4}$ s^{-1}.

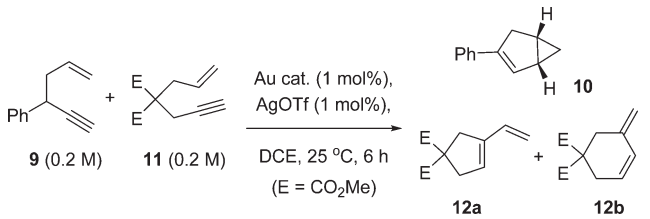

Scheme 3 Competition experiment of a 1,5-enyne **9** and 1,6-enyne **11**. Product **11** derives from **9** and products **12a** and **12b** from **11**. The kinetic profiles are shown in Fig. 6 and product distributions of **12a** : **12b** shown in Fig. 7.

1,5-Enyne **9** (0.2 M) and 1,6-enyne **11** (0.2 M) were subjected to a reaction where the only variable was the Au catalyst {AuBr(I^tPe), $AuBr_2$(*N*-TFS)(I^tPe) and $AuBr_2$(*N*-phthal)(I^tPe)} (Fig. 5 and Table 3). In addition to examining the reactivity difference between **9** and **11**, the experiment allows one to probe the ratio of products formed

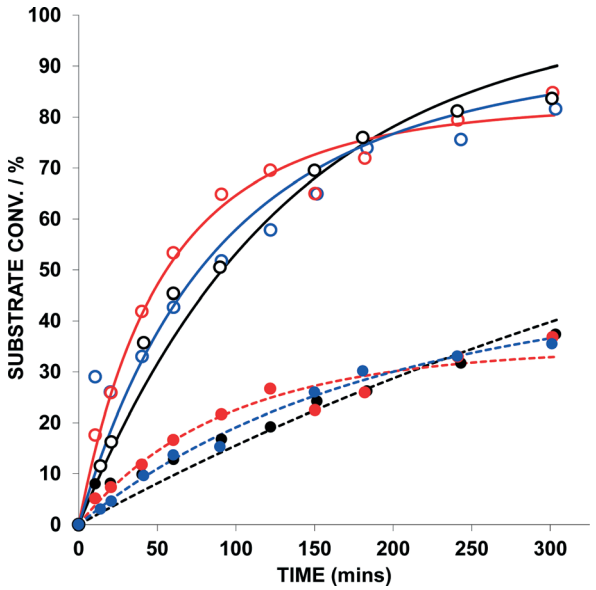

Fig. 5 Kinetic profile for the concurrent cycloisomerisation of 4-phenyl-1-hexen-5-yne (**9**) and dimethyl allylpropargylmalonate (**11**) mediated by selected Au catalysts. Key: 1,5-enyne conversion (**9**, open circles) and 1,6-enyne conversion (**11**, closed circles) – black = AuBr(I^tPe); blue = $AuBr_2$(*N*-TFS)(I^tPe); red = $AuBr_2$(*N*-phthal)(I^tPe). Conditions: 0.2 M **9**, 0.2 M **11** in 1,2-dichloroethane, 1 mol% Au, 1 mol% AgOTf, 25 °C. 1,*n*-enyne (*n* = 5 or 6) conversion monitored by GC analysis – each sample point was quenched by addition of $(n\text{-Bu})_4$NBr. The kinetic curves were fitted using Dynafit™ with standard errors ~ 5%.

in the latter 1,6-enyne cycloisomerization reaction (**12a** : **12b**) as the substrate is consumed over time.

Firstly, AuBr(I^tPe) is a competent catalyst for the cycloisomerization of **11** → **12** ($k_{obs} = 1.08 \times 10^{-4}$ s^{-1}; $T_0 = 2.15 \times 10^{-5}$ moldm^{-3} s^{-1}; standard error = 2.2%). The kinetic analysis of the competition experiments is complicated by the presence of two substrates and two competing catalytic cycles, which is evident in the error analysis. This complication aside, the kinetic profiles are similar in all cases (see Fig. 5). Catalyst performance is reduced for AuBr(I^tPe) as compared to the Au^{III} catalysts – the presence of **12** slows catalytic turnover in the case of AuBr(I^tPe).

A plot of the ratio of **12a** : **12b** over the duration of the 1,6-enyne cycloisomerization reaction, reveals an interesting trend as a function of catalyst (Fig. 6).

Firstly, the independent 1,6-enyne cycloisomerisation of **11** → **12a**/**12b** mediated by AuBr(I^tPe) gives a ratio of *ca.* 1 : 3, which does not alter appreciably over the 6 h reaction time. The same trend is revealed in the competition experiment in the presence of both **9** and **12**, using AuBr(I^tPe) as the catalyst. The product distribution is different for the Au^{III} catalysts, with $AuBr_2$(*N*-TFS)(I^tPe) showing a smaller ratio than $AuBr_2$(*N*-phthal)(I^tPe). Crucially, at *ca.* 1.5 h the ratio of **12a**/**12b** is identical to the AuBr(I^tPe) catalyst. This finding, coupled with our previous observation that dual Au^{III}/Au^I catalyst behaviour is necessary for a successful tandem nucleophilic/1,5-enyne cycloisomerization reaction,[6a] indicates that Au^{III} to Au^I degradation under the working reaction conditions, affects the ratio of products depending on distribution of Au^{III}/Au^I species that are present at any given time. It may be conjectured that liberated *N*-imidate anion could affect the distribution of **12a**/**12b** under the reaction conditions. However, in control experiments we have detected liberation of Br_2 from these Au^{III} catalysts (*see section b, below*).

(b) NMR spectroscopic investigations

NMR spectroscopic analysis allows us to discern whether Au^{III} could be playing a role in the catalysis detailed earlier. It has been suggested previously that Au^{III} can be reduced to Au^I under the reaction conditions.[8] Nolan and co-workers[8a] stated that the active catalyst in the hydration of alkynes and polymerisation of styrene mediated by $AuBr_3$(NHC) type complexes is a Au^I species, formed by reductive elimination of bromide ligands. Further examination of the behaviour of the Au catalysts described herein was deemed necessary, especially whether any evidence for the formation of a cationic Au^{III} catalyst species, and degradation to Au^I, could be gathered.

^{1}H NMR spectroscopy was used to assess whether cationic Au^{III} species were formed by a stoichiometric reaction of $AuBr_2$(*N*-TFS)(I^tPe) with AgOTf in acetone-d_6 (this solvent was selected to increase solubility of all the salts). The I^tPe imidazole proton signals were the most characteristic and sensitive to changes in the Au electronic configuration. It was necessary to compare NMR spectra with reference materials, namely AuBr(I^tPe) and Au(*N*-TFS)(I^tPe), as shown in Fig. 7.

Table 3 Observed rate constants and initial rates for the concurrent cycloisomerization of 1,5-enyne (**9**) and 1,6-enyne (**11**), mediated by selected Au catalysts; data accompanying Fig. 5

Catalyst	$k_{obs} \times 10^{-4}$ (s^{-1})	Rate[a]	Error (%)	Ratio **12a**:**12b**[b]
	1,5-Enyne			
AuBr(I^tPe)	1.27	2.53	5.3	—
$AuBr_2$(*N*-TFS)(I^tPe)	—[c,d]	3.47	2.6	—
$AuBr_2$(*N*-phthal)(I^tPe)	—[e,f]	5.28	4.2	—
	1,6-Enyne			
AuBr(I^tPe)	0.28	0.56	8.4	0.28
AuBr(I^tPe) (1,6-enyne **11** only)	1.08	2.15	2.2	0.30
$AuBr_2$(*N*-TFS)(I^tPe)	—[d,g]	0.85	3.8	0.45
$AuBr_2$(*N*-phthal)(I^tPe)	—[f,h]	1.30	5.6	0.36

[a] Rate at $T_0 \times 10^{-5}$ (moldm^{-3} s^{-1}). [b] After 6 h. [c] Second order k_{1obs} = 8.685 × 10^{-2} mol^{-1} dm^3 s^{-1}. [d] k_{2obs} = 6.38 × 10^{-5} s^{-1} (error 9.2%). [e] Second order k_{1obs} = 0.1321 mol^{-1} dm^3 s^{-1}. [f] k_{2obs} = 1.52 × 10^{-4} s^{-1} (error 8.0%). [g] Second order k_{1obs} = 2.128 × 10^{-2} mol^{-1} dm^3 s^{-1}. [h] Second order k_{1obs} = 3.242 × 10^{-2} mol^{-1} dm^3 s^{-1}.

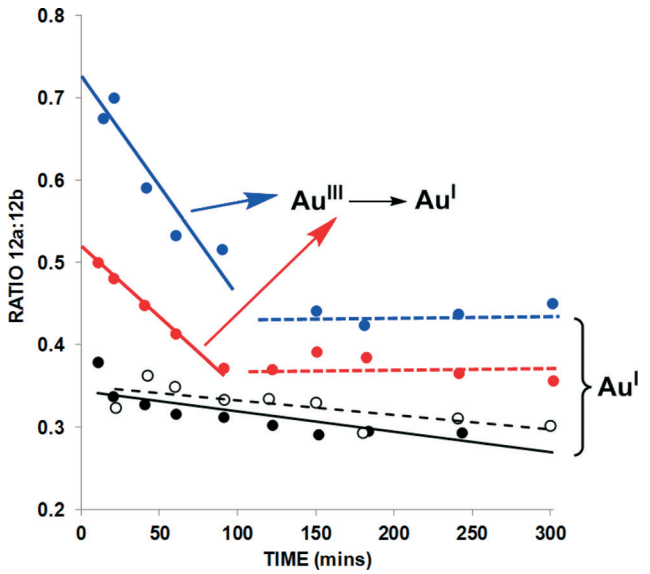

Fig. 6 Product distribution from the cycloisomerization of **11** → **12a** and **12b** over time {data extracted from the kinetic profiles given in Fig. 5 – closed black circles = AuBr(I^tPe); open black circles = AuBr(I^tPe)/1.6-enyne **11** only; closed blue circles = $AuBr_2$(*N*-TFS)(I^tPe); closed red circles = $AuBr_2$(*N*-phthal)(I^tPe)}. The trendlines added to the graph serve as a guide to the eye.

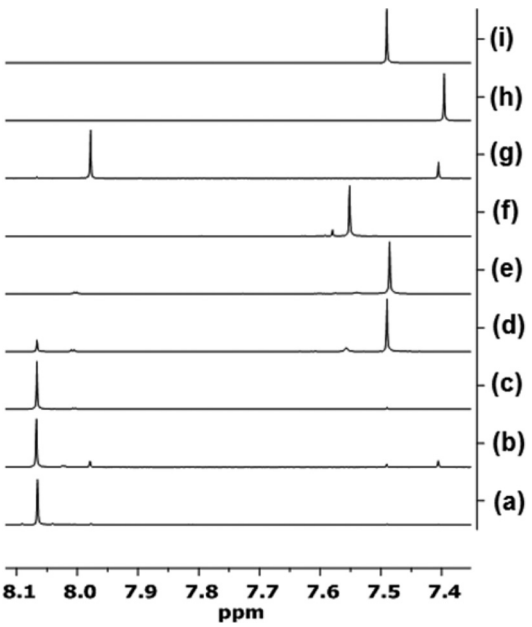

Fig. 7 ^{1}H NMR spectroscopic analysis of the reaction of $AuBr_2$(*N*-TFS)(I^tPe) with AgOTf in acetone-d_6 over time. (a) $AuBr_2$(*N*-TFS)(I^tPe) only; (b) $AuBr_2$(*N*-TFS)(I^tPe), aged for 48 h; (c) $AuBr_2$(*N*-TFS)(I^tPe)/AgOTf (1 : 1), 10 min; (d) as for (c), 4.5 h; (e) as for (c), 22.5 h; (f) AuBr(I^tPe)/AgOTf (1 : 1), 22.5 h; (g) solution of $AuBr_3$(I^tPe) only, aged for 48 h; (h) AuBr(I^tPe) only; (i) Au(*N*-TFS)(I^tPe) only.

The AuBr(I^tPe) imidazole signal shifts 0.15 ppm downfield on treatment with AgOTf, giving Au(OTf)(I^tPe) quantitatively {compare spectra (h) and (f), Fig. 7}. $AuBr_2$(*N*-TFS)(I^tPe) reacts with AgOTf to afford Au(*N*-TFS)(I^tPe) and trace Au(OTf)(I^tPe), with no cationic Au^{III} species observed after 4.5 h {compare spectra (d), (e) and (i)}. The outcome is consistent with the liberation of Br_2 (as noted by a brown colouration). Furthermore, $AuBr_3$(I^tPe) decomposes in solution in the absence of AgOTf, leading to the formation of AuBr(I^tPe) {compare spectra (g) and (h)}. Ageing of $AuBr_2$(*N*-TFS)(I^tPe) led to slow formation of trace but observable amounts of $AuBr_3$(I^tPe), AuBr(I^tPe) and Au(*N*-TFS)(I^tPe) {see spectrum (b)}. The formation of Au(*N*-TFS)(I^tPe) is detected by ^{19}F NMR spectroscopic analysis (see ESI†).

A similar reaction of $AuBr_2$(*N*-TFS)(I^tPe) with Ag[Al(OC(CF_3)$_3$)$_4$] in acetone-d_6 afforded Au(*N*-TFS)(I^tPe) and a new broad signal at slightly higher chemical shift (δ 7.52) which we suggest is [Au(κ^1-O = CMe_2)(I^tPe)]$^+$[Al(OC(CF_3)$_3$)$_4$]$^-$ (see ESI†).

The binding of the $AuBr_2$(*N*-TFS)(I^tPe) and AgOTf toward 1-hexene in CD_2Cl_2 was evaluated to reveal evidence for any alkene–Au^{III} interaction (Table 4), in addition to showing whether liberated Br_2 could be sequestered by 1-hexene. For comparison, the reported spectroscopic data[9] of [Au(μ_2-H_2C = CHC_4H_9)(IPr)][SbF_6] is included in Table 4. A reduction in the alkene proton coupling constants, relative to free 1-hexene, is evidence for π-back donation, *i.e.* an increase in p character for the orbitals at carbon.

The ^{1}H NMR spectral data show no clear evidence for 1-hexene binding to neutral $AuBr_2$(*N*-TFS)(I^tPe), in the absence of AgOTf (Table 4). Upon mixing $AuBr_2$(*N*-TFS)(I^tPe) with 1

Table 4 Binding of 1-hexene to $AuBr_2$(*N*-TFS)(I^tPe) and AgOTf in CD_2Cl_2, as determined by ^1H NMR spectroscopic analysis (400 MHz)

Complex/salt	1-Hexene (equiv.)	δ H_A (ppm)	Coupling constant (Hz)[a]
—	—	5.82	17.0, 10.1, 6.7
AgOTf	2	6.21	17.7, 8.9, 6.6
[$AuBr_2$(*N*-TFS)(I^tPe)]	1	5.82	17.0, 10.1, 6.7
[$AuBr_2$(*N*-TFS)(I^tPe)]/AgOTf	1	6.26	18.0, 8.7, 6.5
[$AuBr_2$(*N*-TFS)(I^tPe)]/AgOTf	2	6.00	17.0, 10.1, 6.7
[Au(μ_2-H_2C = CHC_4H_9)(IPr)][SbF_6]	1	6.05	17, 9, 4.5

[a] The central proton (H_A) was observed as a *ddt*.

equiv. of AgOTf, the solution turns a cloudy colour (due to AgBr formation). Addition of 1-hexene (1 equiv.) results in a shift of $\Delta\delta$ = 0.44 ppm (relative to free 1-hexene). Coupling constants of 18.0 Hz (ΔJ_{E-H} = +1 Hz) for the *trans*-proton and 8.7 Hz (ΔJ_{Z-H} = −1.4 Hz) for the *cis*-coupling were recorded. Addition of 2 equiv. of 1-hexene leads to a reduction in the chemical shift ($\Delta\delta$ = 0.18 ppm), with little change in coupling constants observed. The excess 1-hexene is therefore in exchange with the alkene–Au^{III} species or alkene–Ag^I species. After 24 h, the ^1H NMR spectrum had changed significantly, with a number of small I^tPe imidazole signals corresponding to Au^I and Au^{III} species, in addition to a large broad signal (*ca.* 80% of the total imidazole proton signal) in the Au^I region. Another broad signal at δ 4.45–4.09 ppm was recorded, which we tentatively suggest is the alkene coordinated to Au^I; the broadness in the proton signal is due to fluxionality of the alkene as either Au(μ_2-H_2C = CHC_4H_9)(*N*-TFS)(I^tPe) or the naked cationic species [Au(μ_2-H_2C = CHC_4H_9)(I^tPe)]$^+$. Signals corresponding to free 1-hexene and a new set of proton signals corresponding to 1,2-dibromohexane, *ca.* 50% abundance compared to free 1-hexene, *i.e.* 1 equivalent. After 24 h, there was no evidence of 1-hexene binding to Ag or Au. The ^{19}F NMR spectrum showed a very large broad signal (−182.2 ppm) suggesting the observed alkene complex is that of Au(μ_2-H_2C = CHC_4H_9)(*N*-TFS)(I^tPe). In the absence of 1-hexene, the decomposition of $AuBr_2$(*N*-TFS)(I^tPe) was not observed.

It is important to note that AgOTf alone binds to 1-hexene ($\Delta\delta$ = 0.39 ppm; ΔJ_{E-H} = +0.7 Hz and ΔJ_{Z-H} = −1.2 Hz), which is similar to the binding of $AuBr_2$(*N*-TFS)(I^tPe)/1 equiv. AgOTf. Whilst AgBr is formed, we cannot rule out the involvement of chemical equilibria with $AuBr_2$(*N*-TFS)(I^tPe) and AgOTf. Moreover, under the catalytic conditions there is an excess of substrate and solvent relative to the catalyst system, therefore solubilisation of all the metal species is possible.

(c) Mechanistic discussion

The experimental evidence from this study indicates that AuBr(I^tPe) is the most active catalyst for 1,5-enyne cycloisomerization in the series tested, showing first order behaviour. The Au^{III} catalyst, $AuBr_3$(I^tPe), mediates a slower reaction, which was successfully modelled kinetically as a second order process. The inclusion of a catalyst deactivation step was found necessary for the analysis. The ^1H NMR spectroscopic analysis revealed that $AuBr_3$(I^tPe) degrades to AuBr(I^tBu), even in the absence of AgOTf.

The presence of an *N*-imidate anion led to higher catalyst efficacy (defined as leading to full substrate conversion) in comparison with $AuBr_3$(I^tPe).[10] Of the *N*-imidate series, $AuBr_2$(*N*-TFS)(I^tPe), is the most catalytically active. The nature of the NHC ligand exhibits a significant effect. For example, $AuBr_2$(*N*-phthal)(I^tPe) is twice as active as $AuBr_2$(*N*-phthal)(IMes).

Increasing the 1,5-enyne [**9**], and therefore the concentration of Au catalyst {$AuBr_2$(*N*-phthal)(I^tPe)}, leads to catalyst deactivation. Optimal catalyst performance was recorded at [**9**] between 0.1–0.2 M. At 0.5 M [**9**] it was necessary to model the kinetics to a second order process, again involving a catalyst deactivation step. Product inhibition is also possible at higher concentrations, and formation of Au colloids is visible by the naked eye (purple colouration, relating to the Au plasmon band).

It was possible to assess subtle differences in catalyst behaviour by a concurrent cycloisomerization competition experiment, involving 1,5-enyne **9** and 1,6-enyne **11**. The former gives **10** selectively, whereas **11** afford one of two products, **12a** or **12b**. Three catalysts were tested, namely AuBr(I^tPe), $AuBr_2$(*N*-TFS)(I^tPe) and $AuBr_2$(*N*-phthal)(I^tPe). In all cases, 1,5-enyne **9** was found to be more reactive than 1,6-enyne **11**. Further analysis of the product ratios **12a** : **12b** from the 1,6-enyne cycloisomerization reaction revealed key differences for the Au^{III} catalysts when compared to AuBr(I^tPe). After *ca.* 1.5 h, the ratios of **12a** : **12b** for $AuBr_2$(*N*-TFS)(I^tPe) and $AuBr_2$(*N*-phthal)(I^tPe) mirrored the reaction mediated by AuBr(I^tPe). Therefore, while Au^{III} is still present, **12a** is formed to a greater extent than in reactions solely mediated by Au^I.

Our findings on the 1,5-enyne cycloisomerization process (**9** → **11**) are in-keeping with the DFT calculations reported by Sun and Lin.[5] In that study, it was shown that the 1,5-enyne cycloisomerization reaction mediated by AuCl is both kinetically and thermodynamically favoured for the formation of the bicyclo[3.1.0]hexene product, with key catalytic steps (TS-I_{comp} carbene formation and TS-II_{comp} hydrogen migration) being of similar energy (Scheme 4).

From our experimental findings, we propose that Br_2 is liberated from cationic Au^{III}–NHC catalyst species, affording Au^I–NHC catalyst species *in situ*. The finding is supported by the liberation and trapping of the Br_2 by a sacrificial alkene (1-hexene) in the NMR spectroscopic investigations.

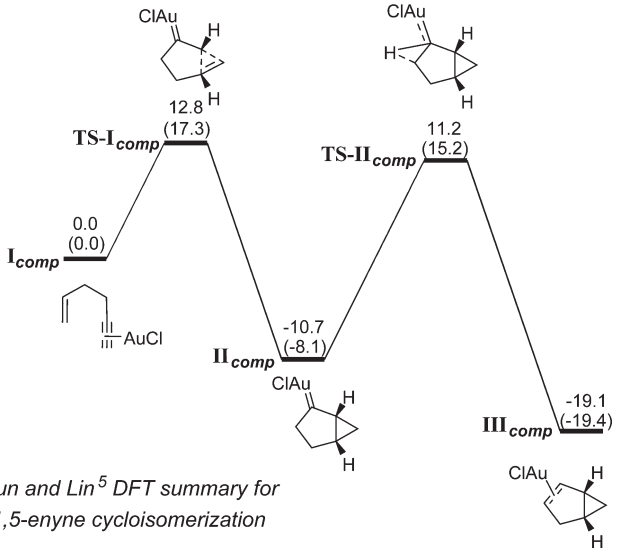

Scheme 4 Top: proposed mechanism for the 1,5-enyne cycloisomerization **9** → **10** (a role for Ag is not shown in the mechanism, although this cannot be ruled out). Bottom: DFT computed energies for the intermediates and transition states for the a 1,5-enyne cycloisomerization mediated by AuCl, reported by Sun and Lin.

Decomposition of the Au^{I}–NHC catalyst species affords Au colloids, which are most likely a moribund-form, especially as reduced catalyst performance is seen at higher [Au] and [**9**] (Scheme 5).

The binding experiments which explored the interaction of 1-hexene with AuBr$_2$(*N*-TFS)(I^{t}Pe)/AgOTf, and AgOTf alone, demonstrates that 1-hexene binding is influenced in both cases. Crucially, 1-hexene mediates the decomposition of AuBr$_2$(*N*-TFS)(I^{t}Pe) to Au(*N*-TFS)(I^{t}Pe), which was not observed in the absence of 1-hexene in CD_2Cl_2. The results taken together demonstrate that unsaturated substrates are involved in: (i) catalyst activation to give Au^{I}, with concomitant decomposition of Au^{III}; (ii) solubilisation of the Ag salt, which is likely non-innocent in the catalysis. Subsequently, the nature of the coordinating ligand (and substrate and any impurities, as shown by substrate-aging experiments) is likely to affect catalytic turnover.

Finally, it is important to emphasise that other products can result from the cycloisomerization of different 1,5-enynes, catalyzed by either AuBr(I^{t}Pe) or AuBr$_2$(*N*-TFS)(I^{t}Pe). In keeping with previous observations,[3a,d] we find that a 1,5-enyne containing a highly substituted carbon tether gives a cyclohexadiene product, both in the tandem nucleophilic substitution-1,5-enyne cycloisomerization (**13** → **14** → **15**) and the latter independent reaction (**14** → **15**) (Scheme 6). The outcome serves to highlight that the catalysts described

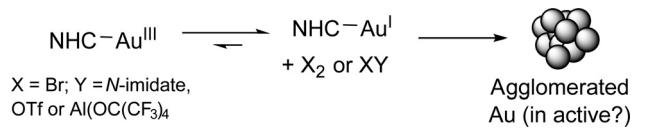

Scheme 5 Catalyst activation and deactivation pathways.

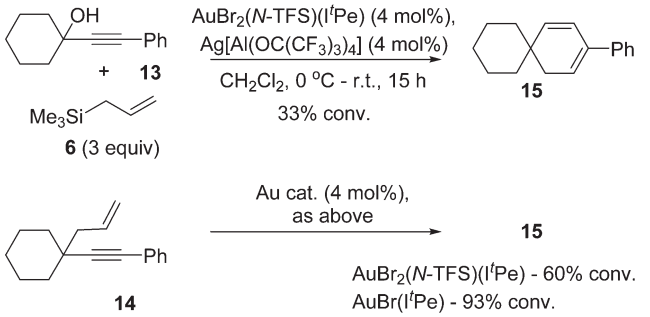

Scheme 6 1,5-Enyne cycloisomerization leading to 1,3-cyclohexadiene formation.

here, and elsewhere, mirror related observations from other studies.

Conclusions

In this paper the ability of both Au^{III} and Au^{I} catalysts to mediate a 1,5-enyne cycloisomerization reaction has been examined. It was necessary to understand whether Au^{III} was being reduced under working catalyst conditions, especially as the success of the tandem nucleophilic substitution-1,5-enyne cycloisomerization relies on Au^{III} for the initial nucleophilic substitution step.[6a]

The reaction kinetics for 1,5-enyne cycloisomerization, mediated by AuBr$_2$(*N*-imidate)(NHC) catalysts {where *N*-imidate = *N*-tetrafluorosuccinimide (*N*-TFS) or *N*-phthalimide (*N*-phthal) and NHC = *N*,*N*′-di-*tert*-pentylimidazol-2-ylidene (I^{t}Pe)}, in the presence of AgOTf, revealed that the nature of the *N*-imidate anionic ligand influences catalyst efficacy. A direct comparison was made with Au^{III}Br$_3$(NHC), which exhibited significant catalyst deactivation in the absence of the stabilizing *N*-imidate ligand. In a concurrent cycloisomerization of 1,5- and 1,6-enynes (**9** and **11**) we were able to tease out subtle differences in the product distribution (**11** → **12a**:**12b**) during the early stages of catalytic turnover by the Au^{III} catalysts. NMR spectroscopic investigations have allowed the ease of reduction of AuBr$_2$(*N*-TFS)(NHC) to Au^{I}X(NHC) (where X = *N*-TFS or Br) to be examined. In these experiments, 1-hexene was shown to mediate Au^{III} decomposition. The liberation of Br_2 from the Au^{III} centre was trapped by this sacrificial alkene.

Taking together all of the results, we conclude, that under working catalyst conditions, cationic Au^{III} is reduced to Au^{I}. The role of Ag^{I} has been more difficult to understand (*i.e.* beyond simple bromide abstraction). The interplay of Au and Ag salts in 1,*n*-enyne cycloisomerization processes is currently being studied within our laboratories.

Experimental

General experimental details

All reactions involving silver salts were carried out in the absence of light. Deuterated and non-deuterated dichloromethane and acetonitrile were dried by passing through a column of activated alumina. Where necessary

dichloromethane Infra-red spectra were recorded on a Unicam Research Series FT-IR spectrometer. Mass spectrometry was carried out using a Fisons Analytical (VG) Autospec instrument. ^{1}H and ^{13}C NMR spectra were collected on a JEOL ECX400 spectrometer operating at 400 and 101 MHz, respectively, and referenced to residual solvent signals. ^{13}C NMR signals are singlets unless otherwise stated. All column chromatography was performed using silica-gel (mesh 220–440) purchased from Fluka Chemicals with the solvent systems specified within the text. TLC analysis was performed using Merck 5554 aluminium backed silica plates, compounds were visualised using UV light (254 nm) and a basic aqueous solution of potassium permanganate. Melting points were measured in open capillary tubes using a Stuart SMP3 Digital Melting Point Apparatus and are uncorrected. 1-Phenyl-2-propyn-1-ol and AgOTf were purchased from Alfa Aesar. All other chemicals were purchased from Sigma-Aldrich Inc. and used without further purification unless otherwise stated. All of the Au catalysts used in this study have been reported; see our previous paper for full details.[6b]

Kinetic experiments

High resolution gas chromatographic (HRGC) analysis. GC was carried out on a Varian 430 instrument with a Factor Four Capillary column (VF-1 ms, 15 m, 0.25 mm) and a flame ionisation detector. Samples of 10 μl were taken *via* syringe from the reaction mixtures at the specified time points. The samples were immediately quenched by addition of the aliquots to a solution of tetra-*n*-butylammonium chloride (8 mM, 20 μl) in CH_2Cl_2. Conversion was determined *via* gas chromatography using a 1 μl sample injected directly into the instrument *via* syringe. Further sampling was carried out on selected aliquots over a period of time to ensure no further conversion occurred after quenching. The errors on the kinetic curves are recorded in the tables detailed in the main text (see also Tables 1–3).

Values for the integrated areas of the GC signals corresponding to starting materials and products were inputted into Microsoft Excel spreadsheet software. This software was used to calculate percent conversions by comparison of starting material and product signal areas. The concentration of the species in solution was determined from the percent conversions and the initial starting material concentration. Selected aliquots were analysed by ^{1}H NMR spectroscopy to ensure consistency with conversions measured by GC.[11]

Kinetic analysis. The reaction kinetics were calculated assuming a first order kinetic model by plotting ln[enyne] against time. Linear least-squares regression was used to calculate observed rate constants, initial rates and standard errors. The calculated concentrations of starting materials and products during the course of the reactions were also inputted into Dynafit™ software (reported by Biokin). Nonlinear least-squares regression was used to fit the experimental kinetic data to predetermined molecular mechanisms as described in the main body of the paper. This was used to determine the order of reaction, observed rate constants, initial rates and standard errors and to fit curves to the kinetic data.

General procedure for the kinetic evaluation of the Au-catalysed cycloisomerization of 4-phenyl-1-hexen-5-yne (9) by gas chromatography

Au complex (3.2 μmol, 0.01 equiv.) and AgOTf (0.8 mg, 3.2 μmol, 0.01 equiv.) were mixed in CH_2Cl_2 (or DCE) in a screw cap vial (1 min) and the solvent removed *in vacuo*. A solution of 4-phenyl-1-hexen-5-yne (**9**) (50.0 mg, 321 μmol, 1 equiv.) in 1,2-dichloroethane (1.60 ml, 0.20 M) was added, the vial sealed with a rubber septum and a positive pressure of argon applied *via* an argon balloon. The mixture was stirred at 25 °C in the absence of light. Samples of 10 μl were taken *via* syringe and added immediately to a solution of tetra-*n*-butylammonium chloride (8 mM, 20 μl) in CH_2Cl_2. Conversion was determined *via* gas chromatography using a 1 μl sample. The chromatogram was run with an injector temperature of 250 °C and an initial oven temperature of 80 °C (0.5 min), heated to 160 °C, at a rate of 20 °C min^{-1}, and maintained at 160 °C (1 min). The retention times were: 2.58 min for 4-phenyl-1-hexen-5-yne (**9**) and 3.89 min for 3-phenylbicyclo[3.1.0]hex-2-ene (**10**).

General procedure for the kinetic evaluation of the Au-catalysed concurrent cycloisomerisation of 4-phenyl-1-hexen-5-yne (9) and dimethyl allylpropargylmalonate (11) by GC. Au complex (3.2 μmol, 0.01 equiv.) and AgOTf (0.8 mg, 3.2 μmol, 0.01 equiv.) were mixed in dichloromethane in a screw cap vial (1 min) and the solvent removed *in vacuo*. A solution of 4-phenyl-1-hexen-5-yne (**9**) (50.0 mg, 321 μmol, 1 equiv.) and dimethyl allylpropargylmalonate (**11**) (67.4 mg, 321 μmol, 1 equiv.) in 1,2-dichloroethane (1.60 ml, 0.20 M) was added, the vial sealed with a rubber septum and a positive pressure of argon applied *via* an argon balloon. The mixture was stirred at 25 °C in the absence of light. Samples of 10 μl were taken *via* syringe and added immediately to a solution of tetra-*n*-butylammonium chloride (8 mM, 20 μl) in CH_2Cl_2 (1 mL). Conversion was determined *via* gas chromatography using a 1 μl sample. The chromatogram was run with an injector temperature of 250 °C and an initial oven temperature of 80 °C (0.5 min), heated to 160 °C, at a rate of 10 °C min^{-1}, and maintained at 160 °C (1 min). The retention times were: 4.04 minutes for 4-phenyl-1-hexen-5-yne (**9**), 7.94 minutes for 3-phenylbicyclo[3.1.0]hex-2-ene (**10**), 5.53 minutes for dimethyl allylpropargylmalonate (**11**), 7.73 minutes for **12a** and 8.15 minutes for **12b**. The ^{1}H and ^{13}C NMR spectroscopic data for **9** and **10** (including representative NMR spectra) have been previously reported.[6]

[(1-Allylcyclohexyl)ethynyl]benzene (14). Prepared by a protocol based on that of Zhan and co-workers.[12] 1-Phenylethynyl cyclohexanol (**13**) (0.50 g, 2.5 mmol, 1 equiv.) and allyltrimethylsilane (**6**) (1.19 ml, 7.5 mmol, 3 equiv.) were mixed in acetonitrile (5 ml, dry) and $FeCl_3$ (anhydrous, 40 mg, 0.25 mmol, 0.1 equiv.) in acetonitrile (1 ml, dry) was added dropwise. The reaction was stirred at 60 °C for 18 h,

reduced *in vacuo* and the product purified by column chromatography on silica gel, eluting with petroleum ether (40–60 °C), to give the title compound as a colourless oil (0.249 g, 1.11 mmol, 44%). ^{1}H NMR (400 MHz, $CDCl_3$) δ 7.44–7.40 (m, 2H), 7.32–7.23 (m, 3H), 6.05 (ddt, J = 12.4, 9.3 and 7.5 Hz, 1H), 5.12 (m, 1H), 5.09 (m, 1H), 2.26 (dt, J = 7.2 and 1.3 Hz, 2H), 1.87–1.58 (m, 7H), 1.28–1.12 (m, 3H). ^{13}C NMR (100 MHz, $CDCl_3$) δ 135.0, 131.6, 128.1, 127.4, 124.2, 117.1, 95.1, 83.3, 47.4, 37.6, 37.0, 26.1, 23.1. ESI+-MS m/z 301.1 (100%, $[M + Ph]^+$), 279.2 (11%), 245.1 (61%), 225.2 (68%, $[MH]^+$), 195.1 (20%), 167.1 (11%), 149.0 (23%), 126.0 (30%). ESI+-HRMS calcd. for $C_{17}H_{21}$ ($[MH]^+$) 225.1638; found 225.1633.

(4,4-Dimethylcyclohexa-1,5-dien-1-yl)benzene (15). [AuBr(I^{t}Pe)] (3.6 mg, 7.4 μmol, 0.02 equiv.), $Ag[Al(OC(CF_3)_3)_4]$ (76) (8.0 mg, 7.4 μmol, 0.02 equiv.) and [(1-allylcyclohexyl)ethynyl]benzene (**14**) (78.3 mg, 0.350 mmol, 1 equiv.) were dissolved in dichloromethane (2 mL) and stirred (0 °C – r.t., 15 h). The reaction mixture was reduced *in vacuo* and purified by column chromatography on silica gel, eluting with petroleum ether (40–60 °C), to give the title compound as a colourless oil (64.8 mg, 0.289 mmol, 83%; 93% conversion noted by NMR). ^{1}H NMR (400 MHz, $CDCl_3$) δ 7.46–7.43 (m, 2H, aromatic CH), 7.39–7.34 (m, 2H, aromatic CH), 7.31–7.26 (m, 1H, aromatic CH), 6.30 (dd, J = 9.9 and 1.8 Hz, 1H, alkene CH d), 6.05 (app. t, J = 4.8 Hz, 1H, alkene CH c), 5.97 (d, J = 9.9 Hz, 1H, alkene CH e), 2.36 (d, J = 4.8 Hz, 2H, CH_2 b), 1.64–1.39 (m, 10H, cyclohexyl CH_2). ^{13}C NMR (100 MHz, $CDCl_3$) δ 140.3 (C), 137.8 (2 peaks, alkene CH e), 134.9 (C), 128.3 (CH), 126.8 (CH), 125.3 (CH), 123.4 (alkene CH d), 122.0 (alkene CH c), 36.3 (broad, cyclohexyl CH_2), 36.2 (alkene CH_2 b), 33.4 (cyclohexyl C), 26.3 (cyclohexyl CH_2), 21.8 (cyclohexyl CH_2). EI+-MS m/z 224 (100%, $[M]^+$), 181 (7%), 167 (34%), 153 (8%), 142 (7%), 115 (6%), 91 (6%), 49 (34%).

NMR experiments

Generation of Au^{III} cationic species from $AuBr_2$(*N*-TFS)(I^{t}Pe) and AgOTf. In acetone-d_6: $AuBr_2$(*N*-TFS)(I^{t}Pe) (10 mg, 1.36×10^{-5} mols) was reacted with AgOTf (3.5 mg, 1.36×10^{-5} mols) in acetone-d_6 (0.67 mL) at 25 °C. The mixture was stirred for 1 h and then a ^{1}H NMR spectrum was recorded (500 MHz). Characterisation details are included in the main body of the text.

In CD_2Cl_2/CD_3CN: $AuBr_2$(*N*-TFS)(I^{t}Pe) (5 mg, 6.8×10^{-6} mols) was reacted with AgOTf (7 mg, 6.8×10^{-6}) or $Ag[Al(OC(CF_3)_3)_4]$ (7.3 mg, 6.8×10^{-6} mols) in CD_2Cl_2 (0.6 mL) and CD_3CN (0.2 mL) at 25 °C. The mixture was stirred for 1 h and then a ^{1}H NMR spectrum was recorded (500 MHz). Characterisation details are included in the main body of the text.

Binding of 1-hexene to $AuBr_2$(*N*-TFS)(I^{t}Pe) and AgOTf, and AgOTf alone. $AuBr_2$(*N*-TFS)(I^{t}Pe) (10 mg, 1.36×10^{-5} mols) was reacted with AgOTf (3.5 mg, 1.36×10^{-5} mols) in CD_2Cl_2 (0.6 mL) for 1 h. Then, 1-hexene (3.4 μL, 2 equiv.) was added and then NMR spectra were recorded (500 MHz). In separate experiments the equivalents of 1-hexene were varied. Characterisation details are included in the main body of the text (Table 4 gives further details). The interaction of AgOTf with 1-hexene was examined on the same scale as above, without the Au^{III} complex. See ESI† for NMR spectral data.

Acknowledgements

We acknowledge GlaxoSmithKline, EPSRC and the Royal Society for funding. Dr J. M. Slattery is thanked for a sample of $Ag[Al(OC(CF_3)_3)_4]$ and discussions concerning this salt. This paper builds on work funded by a previous EPSRC grant (EP/D078776/1).

Notes and references

1 (*a*) A. Arcadi, *Chem. Rev.*, 2008, **108**, 3266–3325; (*b*) Z. Li, C. Brouwer and C. He, *Chem. Rev.*, 2008, **108**, 3239–3265; (*c*) Zigang Li, C. Brouwer and C. He, *Chem. Rev.*, 2008, **108**, 3351–3378; (*d*) E. Jiménez-Núñez and A. M. Echavarren, *Chem. Commun.*, 2007, 333–346.

2 (*a*) Y. Harrak, C. Blaszykowski, M. Bernard, K. Cariou, E. Mainetti, V. Mouriès, A. Dhimane, L. Fensterbank and M. Malacria, *J. Am. Chem. Soc.*, 2004, **126**, 8656–8657; (*b*) M. R. Luzung, J. P. Markham and F. D. Toste, *J. Am. Chem. Soc.*, 2004, **126**, 10858–10859; (*c*) Y. Horino, T. Yamamoto, K. Ueda, S. Kuroda and F. D. Toste, *J. Am. Chem. Soc.*, 2009, **131**, 2809–2811; (*d*) P. Y. Toullec and V. Michelet, *Top. Curr. Chem.*, 2011, **302**, 31–80.

3 (*a*) J. Sun, M. P. Conley, L. Zhang and S. A. Kozmin, *J. Am. Chem. Soc.*, 2006, **128**, 9705–9710; (*b*) L. Zhang and S. A. Kozmin, *J. Am. Chem. Soc.*, 2004, **126**, 11806–11807; (*c*) V. Mamane, T. Gress, H. Krause and A. Fürstner, *J. Am. Chem. Soc.*, 2004, **126**, 8654–8655; (*d*) F. Gagosz, *Org. Lett.*, 2005, **7**, 4129–4132.

4 (*a*) N. Marion, G. Lemière, A. Correa, C. Costabile, R. Ramón, X. Moreau, P. D. Frémont, R. Dahmane, A. Hours, A. Lesage, J. C. Tablet, J. P. Goddard, V. Gandon, L. Cavallo, L. Fensterbank, M. Malacira and S. P. Nolan, *Chem. – Eur. J.*, 2009, **15**, 3243–3260; (*b*) E. Jiménez-Núñez and A. M. Echavarren, *Chem. Rev.*, 2008, **108**, 3326–3350; (*c*) T. Godet and P. Belmont, *Synlett*, 2008, 2513–2517; (*d*) S. M. Ma, S. C. Yu and Z. H. Gu, *Angew. Chem., Int. Ed.*, 2006, **45**, 200–203; (*e*) L. Zhang, J. Sun and S. A. Kozmin, *Adv. Synth. Catal.*, 2006, **348**, 2271–2296; (*f*) C. Nieto-Oberhuber, M. P. Muñoz, E. Buñuel, C. Nevado, D. J. Cárdenas and A. M. Echavarren, *Angew. Chem., Int. Ed.*, 2004, **43**, 2402–2406.

5 T. Fan, X. Chen, J. Sun and Z. Lin, *Organometallics*, 2012, **31**, 4221–4227.

6 (*a*) J. P. Reeds, A. C. Whitwood, M. P. Healy and I. J. S. Fairlamb, *Organometallics*, 2013, **32**, 3108–3120; (*b*) J. P. Reeds, A. C. Whitwood, M. P. Healy and I. J. S. Fairlamb, *Chem. Commun.*, 2010, **46**, 2046–2049.

7 Dynafit program published by Biokin, see: P. Kuzmic, *Anal. Biochem.*, 1996, **237**, 260–273.

8 (*a*) S. Gaillard, A. M. Z. Slawin, A. T. Bonura, E. D. Stevens and S. P. Nolan, *Organometallics*, 2010, **29**, 394–402; (*b*) A. S. K. Hashmi, M. C. Blanco, D. Fischer and J. W. Bats, *Eur. J. Org. Chem.*, 2006, 1387–1389; (*c*) N. Morita and N. Krause, *Eur. J. Org. Chem.*, 2006, 4634–4641; (*d*) S. Komiya and J. K. Kochi, *J. Am. Chem. Soc.*, 1976, **98**, 7599–7607; (*e*) S. Komiya, T. A. Albright, R. Hoffmann and J. K. Kochi, *J. Am. Chem. Soc.*, 1976, **98**, 7255–7265.

9 T. J. Brown, M. G. Dickens and R. A. Widenhoefer, *J. Am. Chem. Soc.*, 2009, **131**, 6350–6351.

10 (*a*) We have seen *N*-imidate ligand effects in catalytic cross-coupling chemistry, see: J. L. Serrano, L. García, J. Pérez, E. Pérez, J. García, G. Sánchez, P. E. Sehnal, S. De Ornellas, T. J. Williams and I. J. S. Fairlamb, *Organometallics*, 2011, **30**, 5095–5109; (*b*) I. J. S. Fairlamb, P. Sehnal and R. J. K. Taylor, *Synthesis*, 2009, 508–510; (*c*) M. J. Burns, I. J. S. Fairlamb, A. R. Kapdi, P. Sehnal and R. J. K. Taylor, *Org. Lett.*, 2007, **9**, 5397–5400; (*d*) C. M. Crawforth, I. J. S. Fairlamb, A. R. Kapdi, J. L. Serrano, R. J. K. Taylor and G. Sanchez, *Adv. Synth. Catal.*, 2006, **348**, 405–412; (*e*) S. Burling, C. M. Crawforth, I. J. S. Fairlamb, A. R. Kapdi, R. J. K. Taylor and A. C. Whitwood, *Tetrahedron*, 2005, **61**, 9736–9751; (*f*) C. M. Crawforth, I. J. S. Fairlamb and R. J. K. Taylor, *Tetrahedron Lett.*, 2004, **45**, 461–465; (*g*) I. J. S. Fairlamb, A. R. Kapdi, A. F. Lee, G. Sánchez, G. López, J. L. Serrano, L. García, J. Pérez and E. Pérez, *Dalton Trans.*, 2004, 3970–3981; (*h*) J. L. Serrano, I. J. S. Fairlamb, G. Sanchez, L. Garcia, J. Perez, J. Vives, G. Lopez, C. M. Crawforth and R. J. K. Taylor, *Eur. J. Inorg. Chem.*, 2004, 2706–2715; (*i*) I. J. S. Fairlamb, A. R. Kapdi, J. M. Lynam, R. J. K. Taylor and A. C. Whitwood, *Tetrahedron*, 2004, **60**, 5711–5718; (*j*) C. M. Crawforth, S. Burling, I. J. S. Fairlamb, R. J. K. Taylor and A. C. Whitwood, *Chem. Commun.*, 2003, 2194–2195.

11 E. H. Niemelä, A. F. Lee and I. J. S. Fairlamb, *Tetrahedron Lett.*, 2004, **45**, 3593–3595.

12 Z. Zhan, J. Yu, H. Liu, Y. Cui, R. Yang, W. Yang and J. Li, *J. Org. Chem.*, 2006, **71**, 8298–8301.